Catalysis Today 164 (2011) 9–15

Contents lists available at ScienceDirect

Catalysis Today

journal homepage: www.elsevier.com/locate/cattod

Surface reduction processes of cerium oxide surfaces by H_2 using ultra accelerated quantum chemical molecular dynamic study

Md. Korshed Alam[a], Farouq Ahmed[b], Ryuji Miura[b], Ai Suzuki[c], Hideyuki Tsuboi[b], Nozomu Hatakeyama[b], Akira Endou[b], Hiromitsu Takaba[a], Momoji Kubo[d], Akira Miyamoto[a,b,c,*]

[a] Department of Chemical Engineering, Graduate School of Engineering, Tohoku University, 6-6-10-205 Aoba, Aramaki, Aoba-ku, Sendai 980-8579, Japan
[b] Department of Applied Chemistry, Graduate School of Engineering, Tohoku University, 6-6-10-205 Aoba, Aramaki, Aoba-ku, Sendai 980-8579, Japan
[c] New Industry Creation Hatchery Center, Tohoku University, 6-6-10-205 Aoba, Aramaki, Aoba-ku, Sendai 980-8579, Japan
[d] Fracture and Reliability Research Institute, Graduate School of Engineering, Tohoku University, 6-6-11-701 Aoba, Sendai 980-8579, Japan

ARTICLE INFO

Article history:
Available online 4 November 2010

Keywords:
UA-QCMD
Hydrogen
Chemical reaction dynamics
Ceria
Catalysts

ABSTRACT

Ceria plays an important role in catalysis, due to its ability to store and release oxygen depending on the condition present in the catalyst environment. To analyze the role of ceria in catalytic reactions it is necessary to know the details of the interaction of ceria surface with environmentally sensitive molecules. This study was conducted using ultra accelerated quantum chemical molecular dynamics UA-QCMD to investigate the reduction processes of the (1 1 1) and (1 1 0) surfaces of ceria with molecular hydrogen as well as water desorption mechanisms from the surfaces. This simulation demonstrated that when high-energy colliding hydrogen's are adsorbed on the ceria, it pulls up an O atom from the ceria surfaces and results in the formation of a H_2O molecule. This is the first time quantum chemical methods have been used for such reduction processes.

1. Introduction

Ceria is important catalysts in various industrial and environmental applications such as a three-way automotive exhaust catalyst (TWC) [1]. Oxygen storage [2], the oxidation of hydrocarbons [3] and CO [4], and decomposition of alcohol [5] and aldehydes [6]. To understand the catalytic properties of both pure ceria and metal/CeO_2 materials, it is imperative to examine the redox surface chemistry. It is capable of oxygen uptake and releases during excursions of the air/fuel mixture into the net oxidizing and reducing regimes, respectively. Recently, these materials have generated great interest in the solid oxide fuel cells as an alternative electrolyte for a lower temperature operation [7,8]. In the related field of "on board" hydrogen production via stream reforming of hydrocarbons, ceria based catalysts are currently being considered to facilitate low temperature water gas shift-gas reaction, which convert CO and water to CO_2 and hydrogen. Most of these technological applications are based on the distinctive feature of Ce ions to easily switch oxidation states between +4 and +3.

To understand the catalytic properties of pure CeO_2 and metal/CeO_2 materials, it is imperative to examine the redox surface chemistry. Defect chemistry of CeO_2 subjected to a H_2 atmosphere has been studied by various experimental techniques; such as temperature programmed reduction (TPR) [9,10] and nuclear magnetic resonance (NMR) [11]. Fierro et al. reported an NMR spectrum, which indicates the incorporation of hydrogen into the cerium oxide when it is heated in a hydrogen atmosphere. The electron spin resonance (ESR) and X-ray diffraction (XRD) also reflect consistent results [12].

Wan et al. demonstrated that the physical effect of nanoparticle sizes on the Ce^{3+} concentration in and the lattice parameter of CeO_2 is stronger than the chemical effect of hydrogen reduction [13]. Al-Madfa et al. studied the kinetics of ceria pellets by electrical conductivity and thermogravimetry techniques [14,15]. In particular, the electrical conductivity transients signified two processes: oxygen desorption and surface reduction. Hydrogen interaction with the Rh deposited onto CeO_2 using X-ray photoelectron spectroscopy (XPS) [16]. Specifically, cerium oxide films were reduced by H_2 exposure if and only if Rh/CeO_2 surfaces were preexposed to gaseous O_2. The interaction of perfect and lightly reduced ceria (1 1 1) surfaces with hydrogen and water molecule have studied using DFT calculations and concluded that rapid dissociation of water at vacancy sites and also predicted a strongly exothermic character for H_2 chemisorption on the ideal ceria (1 1 1) surface [17].

* Corresponding author at: Department of Applied Chemistry, Graduate School of Engineering, Tohoku University, 6-6-10-205 Aoba, Aramaki, Aoba-ku, Sendai 980-8579, Japan. Fax: +81 22 795 7235.
E-mail address: miyamoto@aki.che.tohoku.ac.jp (A. Miyamoto).

0920-5861/$ – see front matter © 2010 Elsevier B.V. All rights reserved.
doi:10.1016/j.cattod.2010.10.011

Vicario et al. [18] provided a sensible description of hydrogen absorption process using DFT. However, their 0 K computational study does not provide any insights on the different possible mechanisms of water desorption, but for the observation that formation of the surface OH groups causes an important protrusion of the H-bonded O atoms and thus the lengthening of the corresponding Ce–O bond, which might be the starting point for water desorption, under the favorable conditions.

Chen et al. [19] reported the reduction mechanisms of CeO_2(1 1 1) and (1 1 0) surfaces by hydrogen using DFT methods. However, the first principles QCMD demand extremely huge computational costs. Our newly developed UA-QCMD method is faster than the conventional first principles method and it can simulate easily complex chemical reaction at reaction temperatures.

In the present study, we applied our in-house code for UA-QCMD to simulate the reduction processes of ceria surfaces. The purpose is to investigate the reduction mechanisms of the ceria surface by hydrogen, which creates oxygen vacancies on the surface and subsequently causes water desorption from the surfaces.

2. Computational methods

2.1. Quantum chemical molecular dynamics method

To investigate the atomic interactions between hydrogen on ceria surfaces, we used our in house code UA-QCMD [20,21]. The program is based on a tight-binding quantum chemistry (TBQC) calculation program "New colors" [22–25] and classical molecular dynamics program "NEW RYUDO" [21,26]. In the UA-QCMD program, the center of the chemical reaction and electrons transfer dynamics are calculated by the new colors program and remaining part is calculated by the new ryudo program, thus realizing the study of chemical reaction and electrons transfer dynamics for a complex system.

Dynamics of atoms were carried out using the following potential functions, which were employed to consider the ionic, covalent, and weak van der Waals interactions among atoms.

$$U = \sum_i \sum_{j>1} \left[\frac{Z_i Z_j e^2}{r_{ij}} + f_0(b_i + b_j)\exp\left(\frac{a_i + a_j + r_{ij}}{b_i + b_j}\right) - \frac{c_i c_j}{r_{ij}^6} \right] + \sum_i \sum_{j>i} D_{ij}\{\exp[-2\beta_{ij}(r_{ij} - r_0)] - 2\exp[-\beta_{ij}(r_{ij} - r_0)]\} \quad (1)$$

The first term corresponds to the Coulomb potential, and the second term corresponds to the short-range exchange repulsion potential (f_0 is the constant for unit adjustment, a is the size, and b is the stiffness), which gives a good account of the repulsive interactions arising from the overlap of electronic clouds. The third term represents van der Waals dispersive interaction (c is the constant for each atom). The fourth term in Eq. (1) corresponds to the Morse-type potential, which represents covalent interactions, where D_{ij} is the bond energy, β_{ij} is the form factor, and r_0 is the bond length at minimum energy. Using these potentials determined by the above-mentioned scheme, a classical molecular dynamics (MD) simulation was performed.

In this MD simulator, a Verlet algorithm [27] is employed to integrate equation of motion. Moreover, the temperature scaling method implemented in the system is similar to the Woodcock algorithm [28].

In the TB-QC, an electronic structure calculation was performed by solving the Schrödinger equation ($\mathbf{HC} = \varepsilon\mathbf{SC}$; **H**, **C**, ε, and **S** refer to the Hamiltonian matrix, eigenvectors, eigenvalues, and overlap integral matrix, respectively) with the diagonalization condition ($\mathbf{C^T SC} = \mathbf{I}$; **I** refers to the identity matrix). In the TB-QC, the double-ζ Slater type basis set was employed and long-range Columbic interactions were computed by the Ewald method [29]. In order to determine the off-diagonal elements of **H**, $\mathbf{H_{rs}}$, the corrected distance-dependent Wolfsberg–Helmholz formula Eq. (2) was used;

$$H_{rs} = \frac{K}{2} S_{rs}(H_{rs} + H_{ss}) \quad (2)$$

Table 1
Determined coefficients of single zeta parameter in Slater type atomic orbital.

Element	AO	a_0	a_1	a_2	a_3	a_4	a_5
H	s	2.000	9.7715	−0.0000	0.0000	0.0000	1.0000
O	s	2.1450	0.0802	0.0185	0.0007	0.0000	0.0000
	p	1.9664	0.5181	1.0817	1.1475	0.0000	0.0000
Ce	s	2.7165	0.0332	0.0208	0.0041	0.0000	0.0000
	p	2.6592	0.0010	−0.0127	0.0093	0.0000	0.0000
	d	3.1519	0.3368	0.0000	0.0000	0.0000	0.0000
	f	4.5582	0.3363	0.0000	0.0000	0.0000	0.0000

2.2. First-principles parameterisation in tight-binding calculation

In order to set the Hamiltonian matrix **H** and overlap integral matrix **S** in our TB-QC simulator which is a part of our UA-QCMD simulator, exponents of a Slater-type atomic orbital (AO), denoted as ζ_r, and valence state ionization potentials (VSIPs) for the 1*s* AO of H atoms as well the 2*s* and 2*p* AOs of O atoms, 4*d* and 4*f* AOs of Ce atoms are necessary. The former parameters are used to calculate the **S** matrix and H_{rs} in Eq. (3). The latter ones are used for the diagonal element of H (H_{rr} or H_{ss} in Eq. (4)). The relationship between H_{rr} and VSIP of *r*-th AO of the *i*-th atom (I_r^i) is described as $H_{rr} = -I_r^i$. In our UA-QCMD simulator, these are represented by the polynomial functions of atomic charges. The ζ_r, and H_{rr} are calculated by the polynomial functions of atomic charges described by Eqs. (3) and (4), respectively.

$$\zeta_r = a_0 + \sum_{k=1}^{5} a_k (Z_i)^k \quad (3)$$

$$H_{rr} = b_0 + \sum_{k=1}^{5} b_k (Z_i)^k \quad (4)$$

In Eqs. (3) and (4), Z_i corresponds to the atomic charge on the atom *i*. The parameters regarding ζ_r, i.e., a_0, a_1, a_2, a_3, a_4, and a_5 in Eq. (3) and regarding H_{rr}, i.e., b_0, b_1, b_2, b_3, b_4, and b_5 in Eq. (4), were determined so as to reproduce the binding energies and electronic structures of a H_2/CeO_2 (1 1 1) surface model was obtained by DFT calculations, which are summarized in Tables 1 and 2, respectively and will be explained later on.

2.3. Periodic density functional theory method

The DFT calculations were also performed in order to validate the accuracy of our TB-QC method. The DMol^3 code [30] was used for the present purpose and double numerical

Table 2
Determined coefficients of H_{rr} parameter.

Element	AO	b_0	b_1	b_2	b_3	b_4	b_5
H	s	−10.5503	−12.4348	−1.4354	0.0000	0.0000	0.0000
O	s	−28.6066	−15.0328	−1.4510	−0.4949	0.0419	0.0000
	p	−14.2851	−14.8159	−1.6244	0.0154	0.0434	0.0000
Ce	s	−5.5303	−5.0728	3.4414	−4.3070	1.5907	−0.1994
	p	−0.0612	−4.6247	3.8922	−4.4481	1.6406	−0.2082
	d	−8.4356	−4.8609	7.5711	−9.4497	3.5251	−0.4442
	f	−7.1929	−8.1663	3.1559	−1.5706	0.0885	0.0000

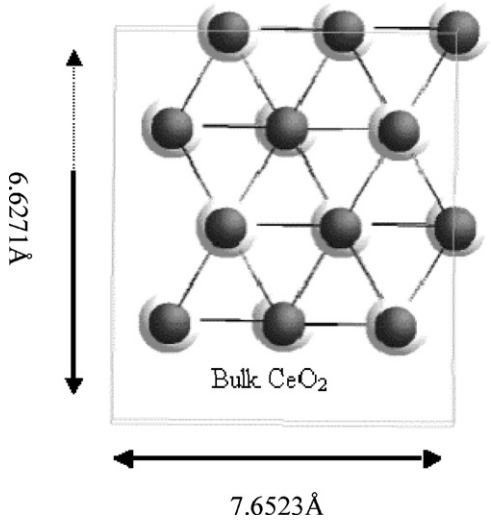

Fig. 1. CeO_2 bulk model (cell parameters: $a = 7.6532$ Å, $b = 6.6271$ Å, $c = 9.372$ Å, and $\alpha = \beta = \gamma = 90^\circ$) was used in the validation of parameterization. Here white sphere represent Ce atom and black sphere represent O atom.

basis sets with polarization functions (DNP) were employed. The parameters used in Eqs. (1) and (2) were tuned comparing with DFT results (atomic charges, bond populations, atomic orbital populations and binding energies). The geometry optimization was performed using the Vosko, Wilk, and Nusair (VWN) local density approximation functional [31] while the energies were recalculated using the generalized gradient approximation (GGA) with Perdew–Burke–Ernzerhof (PBE) exchange-correlation function [32] was adopted for energy calculations. The charge population was analyzed by Hirshfeld method [33].

3. Results and discussion

In order to validate our parameters shown in Tables 1 and 2, a bulk model of CeO_2 cluster was prepared, which was depicted in Fig. 1 CeO_2 model containing 12 cerium and 24 oxygen atoms, was used for the method validation in the present study. By using DMol^3 program we performed geometry optimization of this structure. The accuracy of the used parameters were evidenced by comparison of the atomic charges, atomic orbital populations, bond populations, and total binding energies of the CeO_2 bulk model obtained by TB-QC method and DFT method with different exchange correlation potential. Table 3 shows the comparison of the atomic orbital population of CeO_2 model by DFT and TB methods. From this table it can be clarified that the atomic charges on Ce and O atoms were close to those obtained by DFT. There was no significant difference found in charge values of different atoms calculated by different exchange correlation potential and TB-QC method. Table 4 shows comparison of total binding energy of the system obtained by DFT and by TB-QC. Table 5 shows the comparison of the bond populations for the Ce–O, in CeO_2 bulk model, which agreed well with DFT results.

Table 3
Comparison of atomic orbital population of bulk CeO_2 model by DFT and TB-QC method.

	Charge	s%	p%	d%	f%
DFT					
Ce	0.50	0.30	0.10	1.93	1.17
O	−0.25	1.75	4.50		
TB-QC					
Ce	0.50	0.31	0.10	1.92	1.17
O	−0.25	1.17	4.47		

Table 4
Calculated total binding energy of CeO_2 (bulk model).

System	Binding energy [kcal/mol]	
	DFT	TB
CeO_2	−4144.8	−3990.92

Table 5
Calculated bond population of CeO_2 (bulk model).

	Bond population Ce–O	
	DFT	TB
Ce–O	0.22	0.19

The reduction of the (1 1 1) and (1 1 0) surfaces of ceria by H_2 were calculated as shown in Figs. 2 and 3. The initial interaction of the hydrogen molecule approaching the metal oxide surface is van der Waals attraction. In initial structure the H–H distance is 0.754 Å and the distance between H_2 to O (surf) is 5.47 Å.

Oxygen vacancies are pertinent in the defect chemistry of CeO_2. Oxygen vacancy defect can appear on the oxide surface or in the bulk and can strongly modify the electronic and catalytic properties of the oxide. For a direct observation of the surface and the surface processes at the atomic scale, defect and adsorbates at slightly and strongly reduced ceria, the thermodynamically most stable and easily prepared crystallographic termination of ceria have already been studied by scanning tunneling microscopy (STM) [34,35] and non-contact atomic force microscope (NC-AFM) [36,37]. We have already calculated oxygen vacancy formation energy (E_{vac}) of first layer in the surface using the equation.

$$E_{vac} = E(CeO_{2vac}) + E(O) - E(CeO_2)$$

where $E(CeO_{2vac})$ is the total energy of the slab with the vacancy, $E(CeO_2)$ is the total energy of the slab computed for the stoichiometric slab, and $E(O)$ is the computed binding energy for O atom. The oxygen vacancy formation energy on the surface of ceria was estimated to be −3.87 eV, which is in good agreement with our recent report [21] and previous theoretical investigation [38].

The (1 1 1) and (1 1 0) surfaces of ceria were modeled with super cell slabs consisting of six layers of 26 atoms in the unit cell [39]. The lattice parameters are $a = 6.6271$ Å, $b = 7.6523$ Å, and $c = 20.00$ Å. We used a theoretical equilibrium lattice parameter and the thickness of the vacuum separating the slabs is 11.82 Å. As the initial structure, a single hydrogen molecule was placed on the free surfaces above the Ce and O atoms and the distance between hydrogen and the surface was 5.47 Å. In the present study, a high temperature of 873 K was used and the corresponding mean velocity about 2700 m/s was given to the hydrogen molecule.

Before setting up this velocity for hydrogen molecule, we investigated the effect of different velocities for hydrogen molecule. No adsorption occurred for 1000 m/s of hydrogen molecule and the same phenomena was observed for 2000 m/s and 2500 m/s. For 2700 m/s the hydrogen was completely adsorbed. In case of 3000 m/s the hydrogen molecule was adsorbed on the surface but surface is not stable. So considering the adsorption phenomena and surface stability we set up the velocity 2700 m/s for hydrogen molecule.

To reduce the computational cost we fixed bottom O–Ce–O layers of ceria while upper O–Ce–O layers were relaxed. Simulations were performed at a temperature of 873 K for the models. To determine the position of the adsorbed hydrogen, we have performed full structural relaxations of the slab on which a hydrogen molecule had been positioned on the different initial sites.

Six snapshots taken from the simulations at different time steps are shown in Figs. 2 and 3. In this calculation, we focused

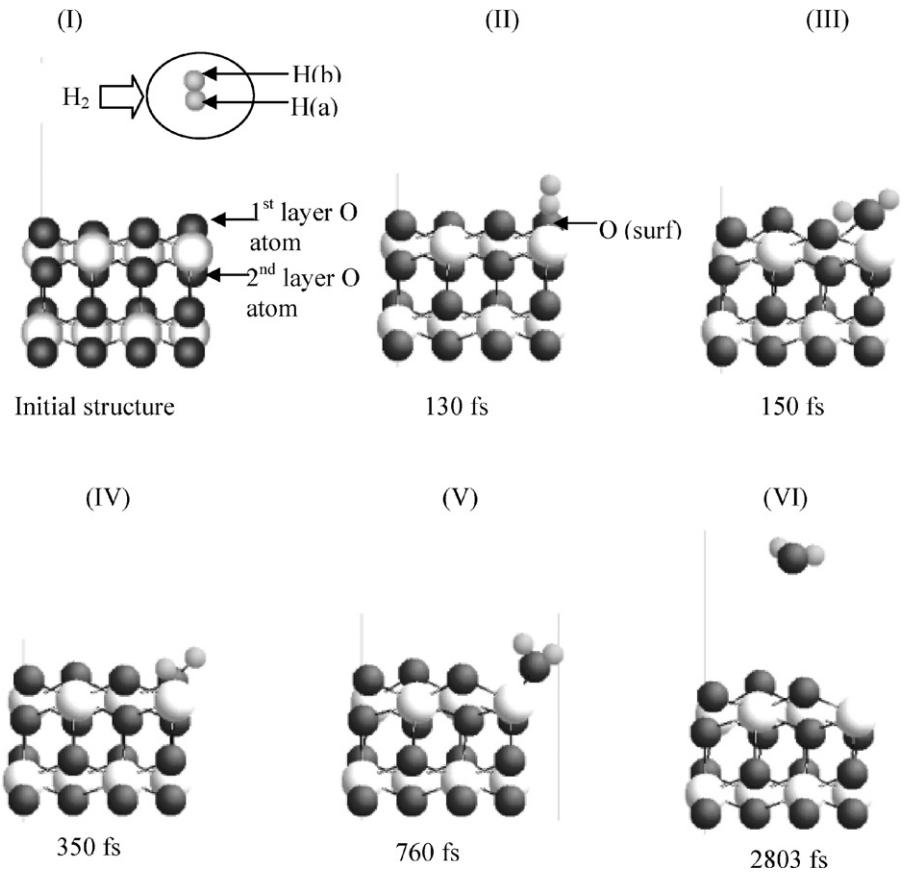

Fig. 2. (I) Initial structure of CeO_2(1 1 1)–H_2 system. Here the black spheres represents O, the white spheres Ce, and the gray spheres H. (II) Snap shot at 130 fs for (1 1 1) surface of ceria, where in the dynamics simulation hydrogen molecule adsorbed on the ceria surfaces. (III) Snap shot at 150 fs, where H_2 interact with the surface. (IV) and (V) where two O–H groups interacting with each other and water molecule about to desorbs from the surface. (VI) Final structure, where an O come out from the surface form H_2O molecule creating oxygen vacancy in the ceria surface.

on three specific atoms H(a), H(b) and surface oxygen (O_{surf}) as shown in Fig. 2. During the simulations, bond lengths, bond energies and structural change were observed to discuss the bond breaking, bond-formation, electron transfer, and structural change at the CeO_2–H_2 interface. According to the MD simulations, initially, hydrogen molecule comes close to the surface as shown in Figs. 2(II) and 3(II). At 130 fs, the hydrogen molecule adsorbed to the O_{surf} atom on the CeO_2 (1 1 1) surface and at 230 fs, H_2 is adsorbed on the CeO_2 (1 1 0) surface as shown in Fig. 3(II). The hydrogen molecule sinks along the normal to the surfaces up to a distance of 1.00 Å on the first atomic layer. The most important geometrical changes (with respect to relaxed clean surfaces) induced by the hydrogen adsorption in both cases involve the O atom directly bonded to hydrogen and the nearest cerium atoms. In the simulations, status of atoms in the relaxed upper layers change respect to time. The adsorption energy is calculated to characterize the strength of bonding of hydrogen on the surfaces and defined as: $E_{ad} = E(CeO_2) + E(H_2) - E(CeO_2 + H_2)$. In this case, the calculated adsorption energies are −28.7 kcal/mol for the (1 1 1) surface at 350 fs and −38.2 kcal/mol for the (1 1 0) surface of ceria at 230 fs, indicating that the adsorption of hydrogen molecule on these surfaces of ceria is energetically favored.

The calculated velocities of the desorbing water are 3240 m/s for the CeO_2(1 1 1) surface and 3020 m/s for the CeO_2(1 1 0) surface. Different velocities of water molecules indicate surface stability and dependency. The fallen potential energies of surfaces during the simulation provide the kinetic energy for desorbing water molecule from the surfaces. According to our results it suggests that (1 1 1) surface is more stable then CeO_2(1 1 0).

Fig. 4 illustrated the change in the bond lengths between the O(surf) and H(a) to H(b) during the simulations. Due to dynamics the atomic status changes respect with time. Finally, the bond distances of O–H(a) and O–H(b) become about 1.00 Å, which indicates that the desorbing molecule is water. This value has good agreement with experimental findings [40].

Fig. 5 shows the changes in the bond energies between O(surf) and to H(a) to H(b). During the UA-QCMD simulation, the values of the bond energies of the O(surf) to H(a) were 0.0, −41.36, −114.71, and −104.07 kcal/mol at 0 fs, 230 fs, 303 fs and 2803 fs, respectively. On the other hand, the bond energies between O(surf) to H(b) were 0.0, −51.72, −115.28, and −98.4 kcal/mol on the same time sequence. This analysis also suggest that bond energies of O(surf) to H(a) and to H(b) were changing during the simulation before desorbing as water molecule as shown in Table 6.

Fig. 6 indicates that the average atomic charge value for each layer of oxygen atoms increases with time. At the beginning of the interaction the drastic charge variation exposes in case of the most reactive oxygen O(surf) atom, that takes part in interaction with adsorbed hydrogen molecule and finally desorbed from the surface. The electro-negativity of this surface oxygen decreases but average atomic charge value of other surface oxygen atoms increases with simulation time.

As a result of the oxygen vacancy, electrons are thought to localize on the cerium ions neighboring the vacancy site in its 4f orbital state, thereby reducing the cerium ions from Ce^{4+} to Ce^{3+} ions and populating a defect state near the bottom of the conduction band [38]. Fig. 8 is the time profile of the atomic charges on Ce atoms in each layer of CeO_2 (1 1 1). The average charges on the O atoms in each O layer of the CeO_2/H_2 systems were ana-

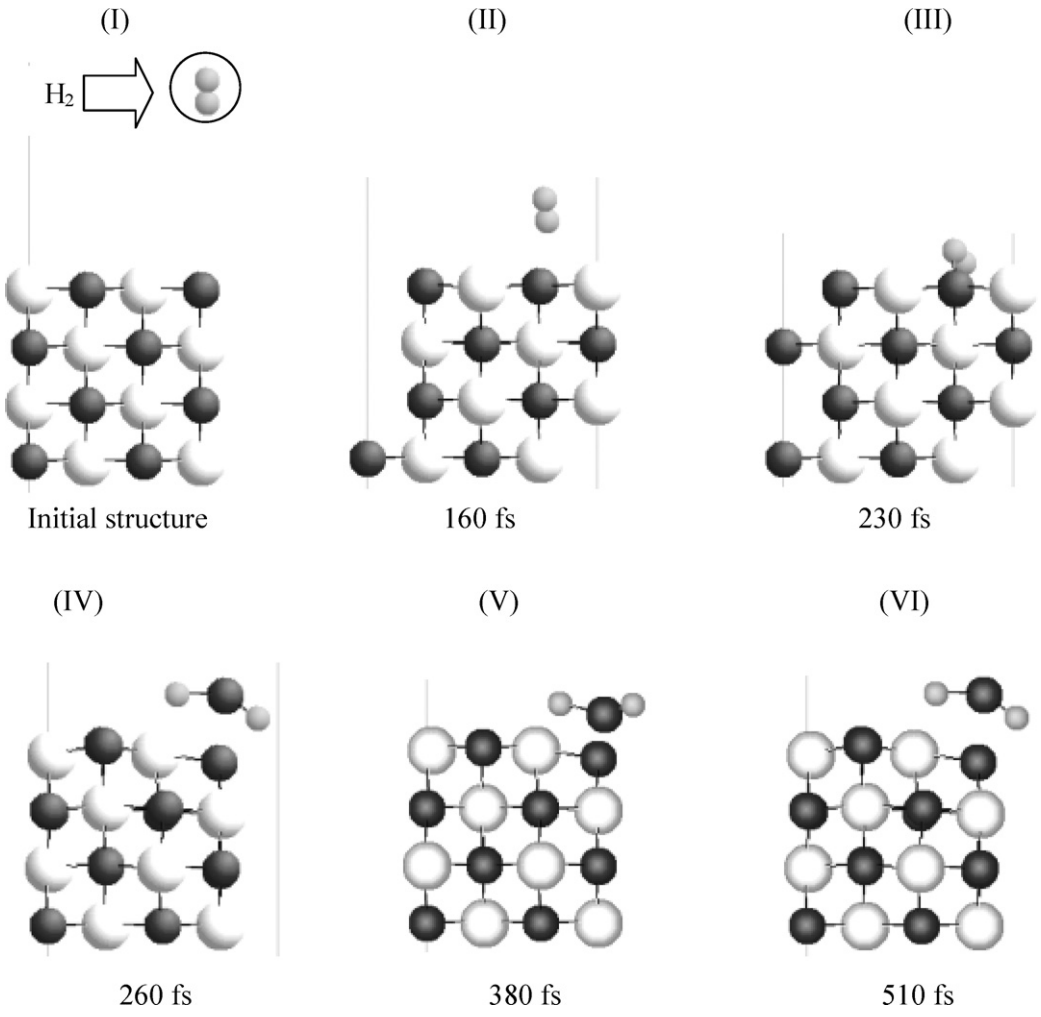

Fig. 3. (I) Initial structure for CeO_2(1 1 0)–H_2 system. Here the black spheres represents oxygen atoms, the white spheres Ce, and the gray spheres H. (II) Snap shot at 160 fs for (1 1 0) surface of ceria, where in the dynamics simulation hydrogen molecule come close to the surface. (III) Snap shot at 230 fs, where hydrogen molecule interacts with the surfaces and hydrogen molecule dissociates followed by the formation of O–H groups. (IV) and (V) where two O–H groups interacting with each other and water molecule about to desorbs from the surface. (VI) Final structure, where an O come out from the surface form H_2O molecule creating oxygen vacancy in the ceria surface.

Table 6
Calculated bond lengths and bond energies of O(surf) to hydrogen atoms [H(a) and H(b)].

Time [fs]	O–H(a)		O–H(b)	
	Bond length [Å]	Bond energy [kcal/mol]	Bond length [Å]	Bond energy [kcal/mol]
0	4.97	0.0	5.73	0.0
230	1.30	−41.36	1.26	−51.72
303	0.89	−114.71	0.88	−115.28
2803	1.05	−104.07	1.10	−98.4

lyzed (Table 7), to study the change of electrons transfer. Here, the employed CeO_2 model consists of four O layers and two Ce layers. The surface and bottom oxygen layers are designated as the first and the fourth O layers respectively, as shown in Table 7. This result indicates that the electron transferred from the hydrogen to Ce and O atoms during the interactions. However, different charge values of Ce atoms in the 1st layer and 2nd layer were observed, as shown in Table 8. Significant charge variation occurred when hydrogen molecule adsorbed on the (1 1 1) at 350 fs and at 230 fs on the (1 1 0) surfaces of ceria. For hydrogen molecule (Table 9), we noticed different charge values with simulation time and significant charge distribution appeared during the simulation as shown in Fig. 7. Initially, average atomic charges on Ce atoms in both layers change but when the water molecule desorbs creating an oxygen

Table 7
Average atomic charges on O atoms in each layer of CeO_2(1 1 1).

	0 fs	100 fs	230 fs	303 fs	1303 fs	2103 fs	2803 fs
1st O layer	−0.982	−0.982	−0.978	−0.938	−0.895	−0.944	−0.938
2nd O layer	−0.893	−0.894	−0.894	−0.942	−0.955	−0.932	−0.932
3rd O layer	−0.898	−0.896	−0.895	−0.923	−0.946	−0.924	−0.925
4th O layer	−0.898	−0.896	−0.895	−0.923	−0.946	−0.924	−0.925

Table 8
Average atomic charges on Ce atoms in each layer of CeO_2(1 1 1).

	0 fs	100 fs	230 fs	303 fs	1303 fs	2103 fs	2803 fs
1st Ce layer	1.876	1.878	1.882	1.893	1.754	1.596	1.669
2nd Ce layer	1.879	1.881	1.883	1.77	1.742	1.959	1.941

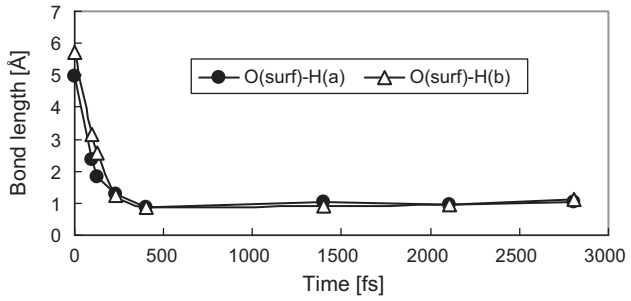

Fig. 4. Change in the bond lengths between hydrogen molecule [H(a) and H(b)] to O(surf) in the ceria observed during the simulation.

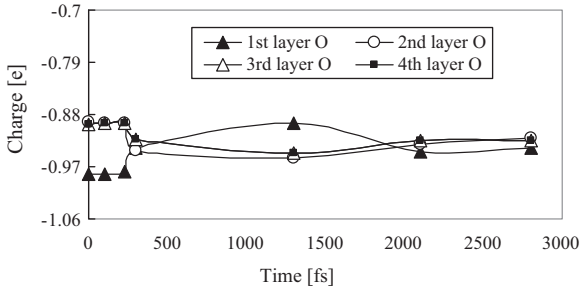

Fig. 5. Change in the bond energies between hydrogen molecule [H(a) and H(b)] to O(surf) atom in the ceria observed during the simulation.

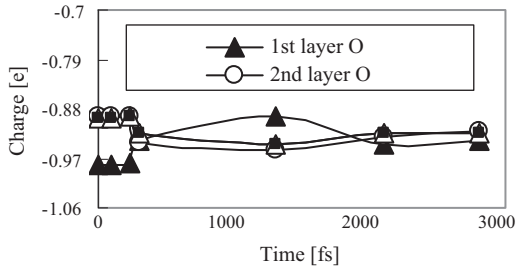

Fig. 6. Time profiles of atomic charges on oxygen atoms in each layer of CeO_2 (1 1 1).

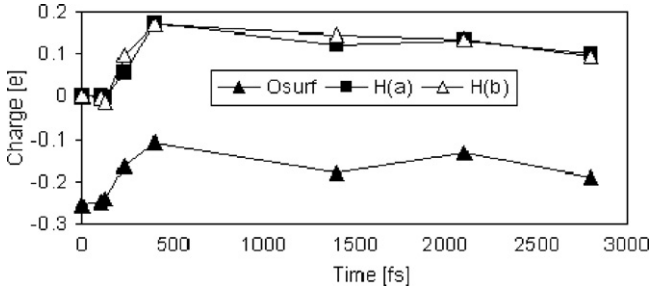

Fig. 7. Atomic charge analysis of hydrogen molecule and O(surf) atom during the simulation (1 1 1).

vacancy on the surface as shown in Fig. 2(VI), the electro-positivity of 1st layer Ce atoms decreased. However, for the 2nd layer, charge value remains approximately constant when compared to the initial structure as mentioned in Table 8. At about 300 fs when the H_2

Table 9
Analyze the atomic charges on H atoms during the MD simulation.

	0 fs	100 fs	230 fs	303 fs	1303 fs	2103 fs	2803 fs
H(a)	0	0	−0.001	0.056	0.172	0.120	0.099
H(b)	0	−0.001	−0.013	0.096	0.169	0.144	0.093

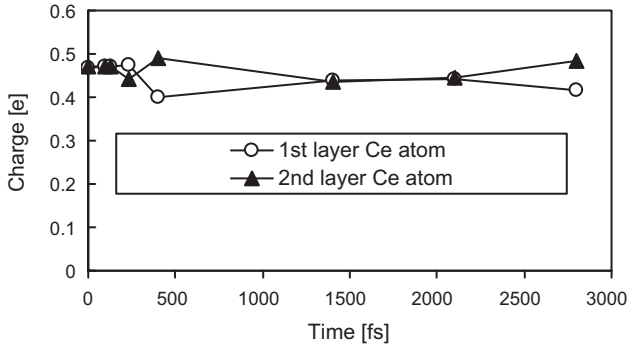

Fig. 8. Time profiles of average atomic charges on Ce atoms in each for CeO_2 (1 1 1).

was adsorbed on the ceria surfaces, a more electro-positivity value was observed for the 1st layer of Ce atoms due to electron transfer from Ce atoms to the hydrogen. Also, massive electrons transfer occurred when the Ce–O bond broke and the O atom reacted with the H_2 molecule, resulting in the desorption of a water molecule. Further detailed analysis show that the electrons were transferred from the *p*-orbital of the O atom to the *f*-orbital of the Ce atom. This reduction reaction is related to the ability of Ce to exist in two oxidation states, Ce^{3+} and Ce^{4+} [41] (Fig. 8).

Adsorbed H_2 species directly dissociates, and the dissociated hydrogen that contain high kinetic energy adsorbed on favorable active O^{-2} sites as shown in Figs. 2 and 3, followed by the formation of OH species. Surface OH species can further diffuse on the reduced CeO_2 surface and interact with each other to produce H_2O, which is accompanied by the reduction of Ce^{4+} to Ce^{3+} and formation of an oxygen vacancy when H_2O desorbs which followed previous theoretical study [18]. Our simulation revealed that the self-containing kinetic energies of adsorbed atom and fallen potential energies contribute to trigger of the desorption of H_2O.

4. Conclusion

This is the first successful simulation of hydrogen molecule on ceria surfaces using our UA-QCMD. It allowed for the investigation of the surface dependency of ceria surfaces on H_2 adsorption on the surface and the velocity of desorbing water. Our calculations results corresponded well to the results from previous experiments. It also revealed more detailed information such as changes in the charge, electronic transfer, variation of bond distances or bond energies and structural change during the simulation. It is also demonstrated that hydrogen molecule which possessed high velocity can reached and interacted with surface oxygen on the active sites of the surfaces and formed O–H groups. Due to mutual interaction between OH groups finally it desorbs as a water molecule. High velocity containing hydrogen molecule and structural change of this system during the simulation provided kinetic energy to complete the desorption process.

References

[1] A.F. Diwell, R.R. Rajaram, H.A. Shaw, T.J. Treux, The role of ceria in three-way catalysts Catalysis Automotive Pollution Control, 71, Elsevier, Amsterdam, 1991.
[2] H.C. Yao, Y.F. Yu Yao, J. Catal. 86 (1984) 254.
[3] (a) L. Kundakovic, M. Flytzani-Stephanopoulos, J. Catal. 179 (1998) 203;
(b) M.J. Tieran, O.E. Finlayson, Appl. Catal. B 19 (1998) 23.
[4] J. Stubenrauch, J.M. Vohs, J. Catal. 159 (1996) 50.
[5] (a) W. Liu, F. Stephanopoulos, J. Catal. 153 (1995) 317;
(b) W. Liu, F. Stephanopoulos, J. Catal. 153 (1995) 304.
[6] (a) H. Idriss, C. Diagne, J.P. Hindermann, A. Kiennmann, M.A. Barteau, J. Catal. 155 (1995) 219;
(b) M.I. Zaki, M.A. Hasan, L. Pasupulately, Langmuir 17 (2001) 768.
[7] T. Hibino, A. Hashimoto, T. Inoue, J. Tokuno, S. Yoshida, M. Sano, Science 288 (2000) 2031.

[8] M. Mogensen, N.M. Sammes, G.A. Tompsett, Solid State Ionics 129 (2000) 63.
[9] E. Aneggi, M. Boaro, C. de Litterbug, G. Dolcetti, A. Trovarelli, J. Alloys Compd. 408 (2006) 1096.
[10] L.A. Bruce, M. Hoang, A.E. Hughes, T.W. Turney, Appl. Catal. A 34 (1996) 351.
[11] J.L.G. Fierro, S. Mendioroz, A.O. Olivan, J. Colloid Interf. Sci. 107 (1985) 60.
[12] J.L.G. Fierro, J. Soria, J. Sanz, J.M. Rojo, J. Solid State Chem. 66 (1987) 154.
[13] X. Wan, D. Goberman, L.L. Shaw, G. Yi, G.M. Chow, Appl. Phys. Lett. 96 (2010) 123108.
[14] H.A. Al-Madfa, M.M. Khader, M.A. Morris, Int. J. Chem. Kinet. 5 (2004) 293.
[15] H.A. Al-Madfa, M.M. Khader, Mater. Chem. Phys. 86 (2004) 180.
[16] J. Xu, S.H. Overbury, J. Catal. 222 (2004) 167.
[17] M.B. Watkins, A.S. Foster, A.L. Shluger, J. Phys. Chem. C 111 (2007) 15337.
[18] G. Vicario, G. Balduuci, S. Fabris, S.D. Gironcoli, S. Baroni, J. Phys. Chem. B 110 (2006) 19380.
[19] H.T. Chen, Y.M. Choi, M. Liu, M.C. Lin, Chemphyschem 8 (2007) 849.
[20] F. Ahmed, M.K. Alam, A. Suzuki, R. Sahnoun, H. Tsuboi, M. Koyama, N. Hatakeyama, A. Endou, H. Takaba, C.A. Del Carpio, M. Kubo, A. Miyamoto, J. Phys. Chem. C 113 (2009) 15676.
[21] Md.K. Alam, F. Ahmed, K. Nakamura, A. Suzuki, R. Sahnoun, H. Tsuboi, M. Koyama, N. Hatakeyama, A. Endou, H. Takaba, C.A. Del Carpio, M. Kubo, A. Miyamoto, J. Phys. Chem. C 113 (2009) 7723.
[22] M. Elanany, P. Selvam, T. Yokosuka, S. Takami, M. Kubo, A. Imamura, A. Miyamoto, J. Phys. Chem. B 107 (2003) 1518.
[23] Y. Luo, Y. Ito, H. Zhong, A. Endou, M. Kubo, S. Manogaran, A. Imamura, A. Miyamoto, Chem. Phys. Lett. 384 (2004) 30.
[24] R. Ishimoto, C. Jung, H. Tsuboi, M. Koyama, A. Endou, M. Kubo, C.A. Del Carpio, A. Miyamoto, Appl. Catal. A 305 (2006) 64.
[25] K. Kasahara, H. Tsuboi, M. Koyama, A. Endou, M. Kubo, C.A. Del Carpio, A. Miyamoto, Electrochem. Solid State Lett. 9 (2006) 490.
[26] T. Onodera, Y. Morita, A. Suzuki, R. Sahnoun, M. Koyama, H. Tsuboi, N. Hatakeyama, A. Endou, H. Takaba, C.A. Del Carpio, M. Kubo, A. Miyamoto, Appl. Surf. Sci. 254 (2008) 7976.
[27] L. Verlet, Phys. Rev. 159 (1967) 98.
[28] L.V. Woodcock, Chem. Phys. Lett. 10 (1971) 257.
[29] P.P. Ewald, Ann. Phys. 64 (1921) 253.
[30] B.J. Delley, Chem. Phys. 113 (2000) 7756.
[31] S.H. Vosko, L. Wilk, M. Nusair, Can. J. Phys. 58 (1980) 1200.
[32] J.P. Perdew, K. Burke, M. Ernzerhof, Phys. Rev. Lett. 77 (1996) 3865.
[33] F.L. Hirshfeld, Theor. Chim. Acta 44 (1977) 129.
[34] F. Esch, S. Fabris, L. Zhou, T. Montini, C. Africh, P. Fornasiero, G. Comelli, R. Rosei, Science 309 (2005) 752.
[35] H. Norenberg, G.A.D. Briggs, Phys. Rev. Lett. 79 (1997) 4222.
[36] Y. Namai, K. Fukui, Y. Iwasawa, Catal. Today 85 (2003) 79.
[37] Y. Namai, K. Fukui, Y. Iwasawa, J. Phys. Chem. B 107 (2003) 11666.
[38] Z. Yang, T.K. Woo, M. Baudin, K. Hermansson, J. Chem. Phys. 120 (2004) 7741.
[39] M. Huang, S. Fabris, J. Phys. Chem. C 112 (2008) 8643.
[40] Z.H. Zhu, G.Q. Finnerty, M.A. Wilson, R.T. Yang, Energy Fuels 16 (2002) 847.
[41] A. Rajendran, Y. Takahashi, M. Koyama, M. Kubo, A. Miyamoto, Appl. Surf. Sci. 244 (2005) 24.